Oxygen Activation at a Dicobalt Centre of a Dipyridylethane Naphthyridine Complex

SCHOLARONE™
Manuscripts

Dalton Transactions

ARTICLE

Oxygen Activation at a Dicobalt Centre of a Dipyridylethane Naphthyridine Complex

Casey N. Brodsky,[a] Guillaume Passard,[a] Andrew M. Ullman,[a] David E. Jaramillo,[a] Eric D. Bloch,[a,b] Michael Huynh,[a] David Gygi,[a] Cyrille Costentin[c] and Daniel G. Nocera*[a]

The mechanism of oxygen activation at a dicobalt bis-μ-hydroxo core is probed by the implementation of synthetic methods to isolate reaction intermediates. Reduction of a dicobalt(III,III) core ligated by the polypyridyl ligand dipyridylethane naphthyridine (DPEN) by two electrons and subsequent protonation results in the release of one water moiety to furnish a dicobalt(II,II) center with an open binding site. This reduced core may be independently isolated by chemical reduction. Variable-temperature ^1H NMR and SQUID magnetometry reveal the reduced dicobalt(II,II) intermediate to consist of two low spin Co(II) centers coupled antiferromagnetically. Binding of O_2 to the open coordination site of the dicobalt(II,II) core results in the production of an oxygen adduct, which is proposed to be a dicobalt(III,III) peroxo. Electrochemical studies show that the addition of two electrons results in cleavage of the O–O bond.

Introduction

Self-healing water splitting catalysts form from the self-assembly of Co [1,2], Mn [3–5] or Ni [6–8] ions in the presence of phosphate (P_i) or borate (B_i) anions. The active sites of the catalysts are metallate clusters with the exemplar CoP_i catalyst exhibiting cluster sizes of ~10 cobalt atoms [9–11]. The OER products of isotopically labelled CoP_i indicate that the mechanism of O–O bond formation proceeds, at least in part, by an intramolecular coupling between oxygens atoms bound to a binuclear cobalt edge site of the cobaltate catalyst. The CoP_i edge site reactivity may be captured by a dimensionally reduced minimal model of a diamond $Co_2(OH)_4$ core stabilized by the six-coordinate dipyridylethane naphthyridine ligand (DPEN) [12]; and the compound has been discussed as a mechanistic model for water splitting by CoP_i [13]. The energy stored in water splitting by the oxygen evolution reaction (OER) may be recovered on demand with a fuel cell thus furnishing a complete fuels cycle [14]. In the case of the dicobalt DPEN molecular system, ORR to H_2O is observed selectively to occur by the $4e^-|4H^+$ PCET reaction when the proton donor pK_a of the system is sufficiently low to result in appreciable driving force [15,16].

[a.] Department of Chemistry and Chemical Biology, Harvard University, Cambridge, Massachusetts 02138, United States. E-mail: dnocera@fas.harvard.edu
[b.] Present Address: Department of Chemistry and Biochemistry, University of Delaware, Newark, Delaware 19716, United States. E-mail: edb@udel.edu
[c.] Laboratoire d'Electrochimie Moléculaire, Unité Mixte de Recherche Université - CNRS N° 7591, Bâtiment Lavoisier, Université Paris Diderot, Sorbonne Paris Cité, 15 rue Jean de Baïf, 75205 Paris Cedex 13, France: cyrille.costentin@univ-paris-diderot.fr
† Electronic Supplementary Information (ESI) available: single crystal X-ray diffraction data; NMR data. See DOI: 10.1039/x0xx00000x

Scheme 1. Dicobalt(III,III) and Dicobalt(II,II) DPEN Complexes.

1 $[Co_2(OH)_2DPEN(\mu-1,3-OC(NH)CH_3)]^{3+}$

2 $[Co_2(OH)DPEN(\mu-1,3-OC(NH)CH_3)]^{2+}$
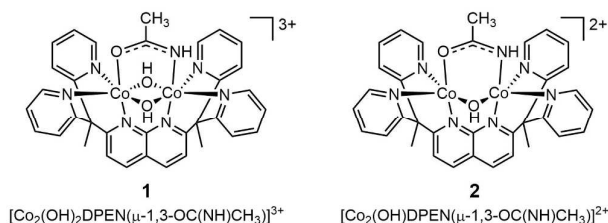
As the OER and ORR reactions may be thought to be the microscopic reverse of each other, ORR may inform on OER and vice versa. Especially important, intermediates unobservable in one reaction may be captured in the reverse reaction. For the case of OER in CoP_i or molecular cobalt model compounds, no oxygen intermediate has yet to be observed. Realizing that the reverse ORR reaction might allow intermediates of relevance to OER at cobalt catalysts to be observed, we turned our attention to the reaction of oxygen at the binuclear site of Co_2-DPEN with the goal of capturing oxygen intermediates. To this end, in this work we utilize an organic-soluble dicobalt complex (**1**, Scheme 1), which is capable of promoting ORR [17]. We implement conditions that allow coordinatively unsaturated intermediates to be isolated and their formation to be examined by a combination of CV, synthetic and spectroscopic techniques. Oxygen binds to a reduced form of **1** to furnish an adduct that is consistent with the formation of a peroxo complex as deduced from chemical reaction studies. Addition of two electrons to this putative peroxo species results in O–O bond cleavage. These results demonstrate peroxo as an intermediate in the O–O bond cleavage of ORR and accordingly may implicate the peroxo as a bond-forming oxygen intermediate in OER at dicobalt centres of CoP_i and associated molecular model complexes.

Figure 1. Solid-state crystal structure of **1**, 50% probability ellipsoids. DPEN hydrogen atoms, solvent molecules, and anions removed for clarity. Selected bond distances: d(Co1–Co2) = 2.658 Å, d(Co1–N1) = 1.897 Å, d(Co2–O1) = 1.907 Å, d(Co1–N2) = 1.906 Å, d(Co1–N3) = 1.901 Å, d(Co1–N4) = 1.945 Å, d(Co2–N5) = 1.932 Å, d(Co2–N6) = 1.902 Å, d(Co2–N7) = 1.900 Å, ∠(Co1–O2–Co2) = 90.374°, ∠(Co1–O3–Co2) = 89.835°.

Results and discussion

Complex **1** was synthesized as previously reported [17] by metallating the dipyridylethane naphthyridine (DPEN) ligand with $Co(NO_3)_2$ in a 1:1 mixture of water and acetone, followed by oxidation to $Co_2(III,III)$ by an excess of H_2O_2, and finally heating in acetonitrile to create the bridging acetamidate ligand. The amide proton is observed in the ^1H NMR spectrum of **1** at 9.1 ppm (Figure S1). Crystals of **1** suitable for X-ray diffraction were obtained by the vapour diffusion of diethyl ether into a solution of **1** in acetonitrile. The resulting solid-state crystal structure of **1**, presented in Figure 1, features a diamond $Co_2(OH)_2$ core with a close Co–Co distance of 2.658 Å.

The CV of **1** in acetonitrile (MeCN), under an inert Ar atmosphere and in the absence of protons, shows a one-electron reversible reduction at –0.012 V vs. NHE (Figure 2a). The heterogeneous electron transfer is fast, as the anodic/cathodic peak separation is consistently 59 mV over a scan rate range from 0.1 to 5 V s^{-1}. The peak height of a such a Nernstian CV wave is [18],

$$i_p = 0.446nFSC\sqrt{\frac{DFv}{RT}} \qquad (1)$$

where n = number of electrons transferred, F = Faraday's constant, S = electrode surface area, D = diffusion coefficient, v = scan rate, and C = substrate concentration. The diffusion coefficient of **1** was determined by diffusion-ordered spectroscopy (DOSY) NMR (Figure S2) to be 8.5×10^{-6} cm^2 s^{-1}. Substituting D into eq. (1) yields as n = 1, establishing that the CV wave in Figure 2 corresponds to the reversible Co(II/III) couple.

Figure 3a shows the change in the CV with the titration of trifluoroacetic acid (TFA, pK_a = 12.6 in MeCN[19]) into a solution of **1** under anaerobic conditions. A loss of reversibility of the CV wave is accompanied by an anodic shift of the peak potential, and an increase in magnitude to twice the integrated current of the Co(II,III) wave (black trace), indicating a two-electron process with the addition of acid. Indeed, this two-electron wave (in strong acid) separates to two one-electron waves in the presence of weaker acid, as shown in
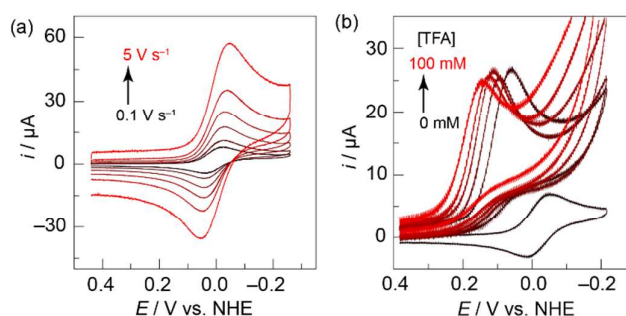
Figure 2. Cyclic voltammogram of **1** (0.5 mM) in MeCN and 0.1 M n-Bu$_4$NPF$_6$ (a) under Ar at scan rates 0.1 (—), 0.2, 0.5, 1, 2, and 5 (—) V s^{-1}, (b) in the presence of 1.62 mM O$_2$ with titration of TFA from 0 (—) to 100 (—) mM at a scan rate of 0.1 V s^{-1}.
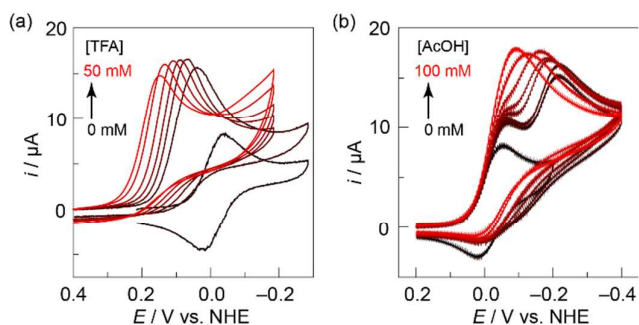
Figure 3. CV of **1** (0.5 mM) in MeCN and 0.1 M n-Bu$_4$NPF$_6$ under Ar in the presence of increasing concentrations of (a) TFA from 0 (—) to 50 (—) mM and (b) AcOH from 0 (—) to 100 (—) mM; v = 0.1 V s^{-1}.

Figure 3b for **1** in the presence of AcOH. Whereas the first reduction wave is invariant with acid concentration, the second reduction wave is broad suggesting a kinetic control by electron transfer but it shifts to more anodic potentials with an increase in acid concentration, suggesting the involvement of a proton transfer upon the addition of the second electron. These observations are consistent with the concomitant transfer of one proton and two electrons to **1** where the transfer of a proton and the second electron are concerted. The E(EC) mechanism for the reduction of **1** in the absence of oxygen is captured by simulations of the CV using DigiElch software [20] for the weak (AcOH) and strong (TFA) acid; as shown in Figure S3, simulated CV waveforms are well-matched to the experimental CVs.

The current of the cathodic CV of **1** in TFA increases upon the addition of O$_2$ (Figure 2b). The CVs do not have the characteristic S-shaped form of a rate-limiting catalytic process, but rather the waveform is peak-shaped, indicating a diffusion-controlled, substrate limiting process [21,22]. The increase of i_p(ORR) over i_p(**1**) by a factor of ~4 implies that **1** binds and activates O$_2$ in the presence of acid in an overall four electron process (*vide infra*).

Synthetic Isolation of Reaction Intermediates. The doubly reduced, singly protonated compound implied by the CVs in Figure 3 was isolated synthetically. A stoichiometric quantity of
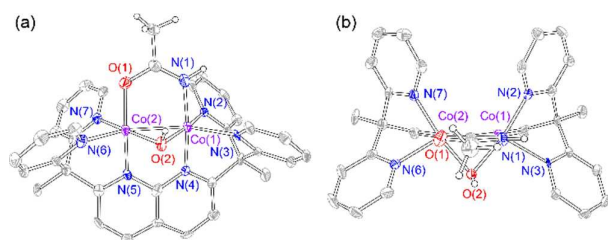
Figure 4. Solid-state crystal structure of **2**, 50% probability ellipsoids. DPEN hydrogen atoms, solvent molecules, and anions removed for clarity. Selected bond distances: d(Co1–Co2) = 2.438 Å, d(Co1–N1) = 1.905 Å, d(Co2–O1) = 1.907 Å, d(Co1–N2) = 1.915 Å, d(Co1–N3) = 2.032 Å, d(Co1–N4) = 1.927 Å, d(Co2–N5) = 1.917 Å, d(Co2–N6) = 2.008 Å, d(Co2–N7) = 1.921 Å, $\angle$(Co1–O2–Co2) = 80.400°.

lithium triethylborohydride (LiHBEt$_3$, superhydride) was added dropwise to a solution of **1** in DMF, and over the course of two days the solution changed from orange to dark green. The reduced compound (**2**) could also be obtained by the reduction of **1** with two equivalents of decamethylcobaltocene in the presence of one equivalent of protonated DMF. Dark green crystals of **2** suitable for X-ray diffraction were obtained by vapour diffusion of diethyl ether into MeCN. The structure of **2**, shown in Figure 4, indicates that one bridging hydroxo moiety is lost upon reduction of the Co$_2$(III,III) core with two Co–N distances increasing from ~1.9 to ~2.0 Å and a decrease in the Co–Co distance from 2.658 Å in **1** to 2.438 Å in **2**.

The ^{1}H NMR of **2** exhibits sharp peaks but is paramagnetically shifted as compared to that of **1** (Figure S1). The paramagnetism of the complex was probed with variable temperature ^{1}H NMR (Figures 5a and 5b). As the temperature is increased from 25 to 85 °C, all peaks broaden and the peak at 6.6 ppm, assigned to the acetamidate N–H proton, is paramagnetically shifted upfield. This observation is consistent with thermal population of the triplet ferromagnetically coupled state from a singlet ground state of **2**, arising from antiferromagnetic coupling within the Co$_2$(II,II) centre. The energy separation between the singlet and triplet states (ΔE_{T-S}) may be determined from fitting the N–H proton paramagnetic shift versus temperature according to eq. 3 [23,24],

$$\delta \text{ (ppm)} = \delta_{\text{singlet}} + 10^6 \frac{g\beta_e}{g_N\beta_N} \frac{aS(S+1)}{kT} \times \left[3 + \exp\left(\frac{\Delta E_{T-S}}{RT}\right)\right]^{-1} \quad (3)$$

A ΔE_{T-S} of 11.01 kJ/mol (919 cm^{-1}) is obtained from fitting eq. (3) (Figure 5b). From this energy separation, the population of the triplet state, as may be determined from the Boltzmann distribution,

$$\frac{N_T}{N_S} = 3 \exp\left(\frac{-\Delta E_{T-S}}{kT}\right) \quad (4)$$
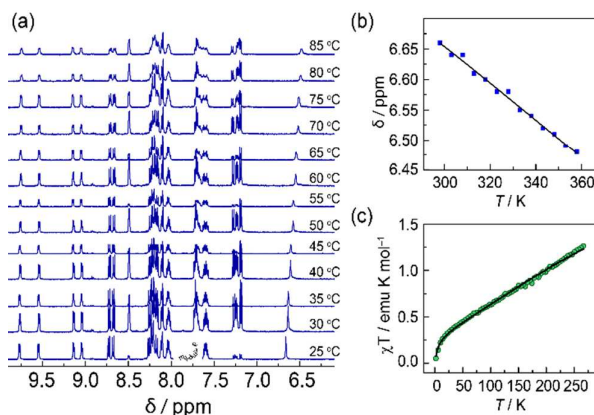
Figure 5. (a) Variable temperature (VT) ^{1}H NMR of **2** in DMSO-d_6, from 25 to 85 °C. (b) NMR shift of the acetamide N–H proton versus temperature (blue squares) with a curvilinear fit to eq 3 (black line). (c) SQUID magnetometry for a solid sample of **2**, fit to eq 5.
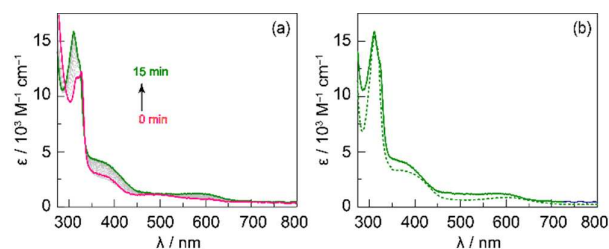
Figure 6. (a) Spectroelectrochemistry of **1** in MeCN (1 mM) in the presence of TFA (1.5 mM), under an applied potential of –0.4 V vs. NHE. (b) UV-vis absorption spectra of chemically and electrochemically reduced **1**: chemical reduction (**2**) in DMF (dotted green trace) and the final spectrum obtained in spectroelectrochemistry (solid green trace) in DMF.

is 3.5% triplet state at room temperature. An independent measure of ΔE_{T-S} was provided by SQUID magnetometry measurements (Figure 5c) of **2**. Fitting χT plots with the Hamiltonian,

$$\widehat{H} = -J\hat{S}_A \cdot \hat{S}_B + \beta\left(\hat{S}_A \cdot g_A + \hat{S}_B \cdot g_B\right) \cdot B \quad (5)$$

using the PHI software package [25], yields a ΔE_{T-S} of 10.67 kJ/mol (892 cm^{-1}) [26], which agrees well with the energy separation measured from VT NMR data.

To correlate the chemical reduction and electrochemical reductions, spectroelectrochemistry was performed on the electrochemical reduction of **1** (Figure 6a). In the presence of a slight excess of TFA and an applied cathodic potential of –0.4 V vs. NHE, the spectrum of **1** converts in 15 min to the spectrum shown in green. This spectrum is consistent with that of the chemically reduced compound **2** (Figure 6b) confirming that chemically isolated **2** represents the same product obtained in anaerobic electrochemical reduction in the presence of TFA. Thus the reduction (electrochemical and chemical) of **1** in the presence of acid is consistent with the following reaction sequence,
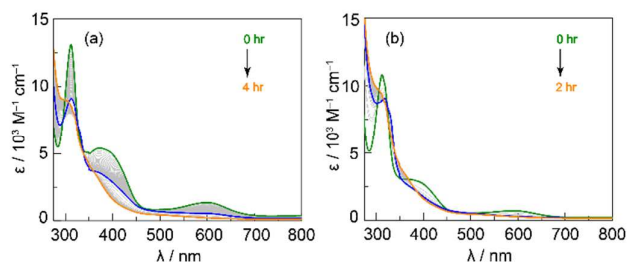
Figure 7. UV-vis absorption spectra of O_2 binding (a) to **2** in DMF and (b) to electrochemically reduced **1** in DMF.
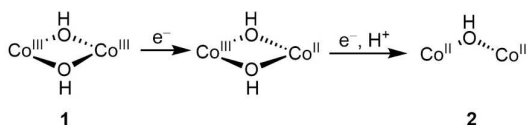
The ability to isolate the two-electron and coordinatively unsaturated intermediate **2** presents a unique opportunity to examine ORR intermediates. When a solution of **2** in DMF is exposed to O_2 at room temperature, the solution changes from dark green to orange over the course of 4 h, as followed by UV-vis absorption spectroscopy in Figure 7a. In the first three hours, the spectrum exhibits an overall decrease in intensity with clear isosbestic points to yield an intermediate with bands at 370 and 420 nm (Figure 7a, blue trace). This intermediate cleanly converts in 1 h to the final spectrum of compound **3**, which exhibits a band at 360 nm (Figure 7a, orange trace); in DMSO, the intermediate with two bands is observed after 5 h and is stable without conversion to the final product (i.e. orange spectrum). The same final spectrum was also obtained by electrochemically reducing **1** in the presence of TFA in DMF by bulk electrolysis at –0.4 V vs. NHE followed by the addition of O_2 (Figure 7b); the low overpotential allows ORR to be arrested and **3** obtained. Additionally, the spectrum of **3** was obtained by the direct reaction of **1** in DMF with 20 equiv of urea hydrogen peroxide (UHP) at room temperature for 1 h (Figure S6); UHP provides a direct source of peroxide as well as protons, in the absence of water. Compound **3** may be obtained as a solid by removing DMF *in vacuo* and dissolving the orange solid in MeCN, followed by vapour diffusion of diethyl ether into the MeCN solution. Crystals of **3** were obtained but did not diffract. The ^{1}H NMR of **3** appears as a diamagnetic compound and its spectrum is very similar to the diamagnetic $Co_2(III,III)$ **1** species (Figure S1). As observed by UV-is spectroscopy, ^{1}H NMR (Figure S4) shows conversion of **2** to **3** in 5 h. In the absence of protons, CV measurements on the intermediate under inert N_2 conditions. A reversible one electron reduction peak is observed at –0.006 V vs. NHE. When TFA is added to solution, the reduction becomes irreversible and the wave shifts anodically (Figure S7a), consistent with breaking an O–O bond. The overall CV and this anodic shift of **3** in the presence of TFA is similar to that obtained for the CV of **1** under ORR conditions of TFA *and* O_2 (Figure S7b).

That **3** can be obtained independently by direct reaction of **1** with UHP is in line with the speciation of **3** as a $Co_2(III,III)$ peroxo. X-ray photoelectron spectroscopy (XPS) spectra are

consistent with a $Co_2(III,III)$ centre for **3**. Figure S5 shows the Co 2p spectrum for complex **3** alongside those of **1** and **2** as authentic $Co_2(III,III)$ and $Co_2(II,II)$ samples, respectively. The edge shift of **3** matches that of **1**. Moreover, the characteristic broad "shake-up" satellite features [27] at higher binding energies in **2** at ca. 786 and 803 eV are absent in **3**. Characterization of the vibrational spectrum of the adduct is obviated by intense vibrations associated with the ligand. Peroxide O–O stretches appear between 700–1000 cm^{-1} [28], but any possible vibrational signatures in this region are obscured by intense ligand stretches, most prominently appearing at 840 cm^{-1} [29].

Density functional theory (DFT) calculations with the B3LYP functional and 6-311G(d,p) basis set in an implicit CPCM acetonitrile solvation environment support a stable μ-η^1-η^1-peroxo-$Co_2(III,III)$ complex (Figure S8). To determine the binding orientation of the nonplanar peroxo, configurations with the O_2 unit pointing upwards towards either the acetamide N or O were evaluated with the former structure slightly lower in energy by 2.9 kJ/mol, suggesting that both configurations are viable at room temperature.

On the basis of the absorption spectrum of the dicobalt O_2 adduct **3** would appear to be most closely aligned to a μ-η^1-η^1-peroxo with a nonplanar Co–O–O–Co unit [30–33] as suggested by the DFT calculations. The UV-vis absorption spectra of such μ-η^1-η^1-peroxos exhibit a weak band in the 300–400 nm region, attributed to the $O_2^{2-}(\pi^*)$ to metal-based orbital LMCT transition, broadened by the excitation of multiple vibrational modes. The putative peroxo species, shows a band at 360 nm with an extinction coefficient of ~2500 M^{-1} cm^{-1}, to relevant literature values. Bipyridine ligated dicobalt centers bridged by a cis μ-η^1-η^1-peroxo and a hydroxide are characterized by a 390 nm absorption band [33–35]. Systems that do not bear a hydroxo moiety but do possess a structurally characterized μ-η^1-η^1-peroxo spanning two dicobalt centers show a bands in the 350-370 nm spectral region [36,37]. In the latter work, the electronic properties of a bridging acetate ligand, akin to the bridging acetamide in this work, cause a red shift in the LMCT absorption of the peroxo. As the electron donicity of the bridging ligand is attenuated the band shifts from 350 nm (7700 M^{-1} cm^{-1}) to 370 nm (9700 M^{-1} cm^{-1}). The acetate compound, which is most similar to the acetamide, shows an absorbance of 350 nm for the peroxo LMCT.

Conclusions

Dicobalt dipyridylethane naphthyridine (DPEN) is a dimensionally reduced minimalist model of the self-healing CoP_i water-splitting catalyst. The complex has captured the edge site equilibrium reactions involving P_i that deliver the open coordination sites needed for the intramolecular O—O bond forming reaction of CoP_i as identified by ^{18}O isotope studies [12]. The open edge coordination site has been shown here in the dicobalt model to support the binding of O_2, leading to O—O bond cleavage. Inasmuch as the O—O bond forming of OER is the microscopic reverse of O—O bond

breaking of ORR, our results suggest that peroxo species may be possible in the OER chemistry of CoPi.

Conflicts of interest

The authors have no conflicts to declare.

Acknowledgements

Notes and references

1   M. W. Kanan and D. G. Nocera, *Science*, 2008, **321**, 1072.
2   Y. Surendranath, M. W. Kanan and D. G. Nocera, *J. Am. Chem. Soc.*, 2010, **132**, 16501.
3   M. Huynh, D. K. Bediako and D. G. Nocera, *J. Am. Chem. Soc.*, 2014, **136**, 6002.
4   M. Huynh, C. Shi, S. J. L. Billinge and D. G. Nocera*, J. Am. Chem. Soc.*, 2015, **137**, 14887.
5   M. Huynh, T. Ozel, C. Liu, E. C. Lau and D. G. Nocera, *Chem. Sci.* 2017, **8**, 4779.
6   M. Dincă, Y. Surendranath and D. G. Nocera, *Proc. Natl. Acad. Sci. U.S.A.,* 2010, **107**, 10337.
7   D. K. Bediako, B. Lassalle-Kaiser, Y. Surendranath, J. Yano, V. K. Yachandra and D. G. Nocera. *J. Am. Chem. Soc.*, 2012, **134**, 6801.
8   D. K. Bediako, Y. Surendranath and D. G. Nocera, *J. Am. Chem. Soc.*, 2013, **135**, 3662.
9   P. Du, O. Kokhan, K. W. Chapman, P. J. Chupas, D. M. Tiede, *J. Am. Chem. Soc*., 2012, **134**, 11096.
10 M. W. Kanan, J. Yano, Y. Surendranath, M. Dincă, V. K. Yachandra and D. G. Nocera, *J. Am. Chem. Soc.*, 2010, **132**, 13692.
11 C. L. Farrow, D. K. Bediako, Y. Surendranath, D. G. Nocera and S. J. L. Billinge*, J. Am. Chem. Soc.*, 2013, **135**, 6403.
12 A. M. Ullman, C. N. Brodsky, N. Li, S. L. Zheng and D. G. Nocera, *J. Am. Chem. Soc.*, 2016, **138**, 4229.
13 T. C. Davenport, H. S. Ahn, M. S. Ziegler and T. D. Tilley, *Chem. Commun.*, 2014, **50**, 6326.
14 N. S. Lewis and D. G. Nocera, *Proc. Natl. Acad. Sci. U.S.A.*, 2006, **103**, 15729.
15 C. T. Carver, B. D. Matson and J. M. Mayer, *J. Am. Chem. Soc.*, 2012, **134**, 5444.
16 J. Rosenthal and D. G. Nocera, *Acc. Chem. Res.*, 2007, **40**, 543.
17 G. Passard, A. M. Ullman, C. N. Brodsky and D. G. Nocera, *J. Am. Chem. Soc.*, 2016, **138**, 2925.
18 J.-M. Savéant, *Elements of Molecular and Biomolecular Electrochemistry: An Electrochemical Approach to Electron Transfer Chemistry*, John Wiley: Hoboken, NJ, 2006.
19 K. Izutsu, *Acid-Base Dissociation Constants in Dipolar Aprotic Solvents*, Blackwell: Boston, 1990.
20 M. Rudolph, *J. Electroanal. Chem.* **2003**, *543*, 23.
21 Rountree, E. S.; McCarthy, B. D.; Eisenhart T. T.; Dempsey, J. L. *Inorg. Chem.* 2014, **53**, 9983.
22 Costentin, C.; Saveant, J.-M. *ChemElectroChem*, 2014, **1**, 1226.
23 B. Le Guennic, T. Floyd, B. R. Galan, J. Autschbach and J. B. Keister, *Inorg. Chem.*, 2009, **48**, 5504.
24 C. M. Lemon, M. Huynh, A. G. Maher, B. L. Anderson, E. D. Bloch, D. C. Powers and D. G. Nocera, *Angew. Chem. Int. Ed.*, 2016, **55**, 2176.
25 N. F. Chilton, R. P. Anderson, L. D. Turner, A. Soncini and K. S. Murray, *J. Comput. Chem.*, 2013, **34**, 1164.
26 G. E. Alliger, P. Mueller, L. H. Do, C. C. Cummins and D. G. Nocera, *Inorg. Chem*., 2011, **50**, 4107.
27 Y. G. Borod'ko, S. I. Vetchinkin, S. L. Zimont, I. N. Ivleva and Y. M. Shul'ga, *Chem. Phys. Lett.*, 1976, **42**, 264.
28 P. Vanelderen, R. G. Hadt, P. J. Smeets, E. I. Solomon, R. A. Schoonheydt and B. F. Sels, *J. Catal*., 2011, **84**, 157.
29 A. L. Gavrilova, C. J. Qin, R. D. Sommer, A. L. Rheingold and B. Bosnich, *J. Am. Chem. Soc.*, 2002, **124**, 1714.
30 P. L. Holland, *Dalton Trans*., **2010**, *39*, 5415.
31 A. E. Martell, *Acc. Chem. Res.*, **1982**, *15*, 155.
32 L. Vaska, *Acc. Chem. Res.*, 1976, **9**, 175.
33 H.-Y. Wang, E. Mijangos, S. Ott and A. Thapper, *Angew. Chem. Int. Ed.*, 2014, **53**, 14499.
34 R. F. Bogucki, G. McLendon, A. e. Martell, *J. Am. Chem. Soc.* **1976**, *98*, 3202.
35 C. Ludovici, R. Fröhlich, K. Vogtt, B. Mamat, M. Lübben, *Eur. J. Biochem.* **2002**, *269*, 2630.
36 R. Köferstein, C. Robl, *Z. Anorg. Allg. Chem.*, **2016**, *642*, 560.
37 M. S. Vad, F. B. Johansson, R. K. Seidler-Egdal, J. E. McGrady, S. M. Novikov, S. I. Bozhevolnyi, A. D. Bond, C. J. McKenzie, *Dalton Trans*., **2013**, *42*, 9921.